Research Paper

Advances in Structural Engineering

Advances in Structural Engineering
2020, Vol. 23(16) 3525–3540

DOI: 10.1177/1369433220939213
journals.sagepub.com/home/ase
SAGE

Seismic retrofit of structures using rotational friction dampers with restoring force

Asad Naeem[1] and Jinkoo Kim[2]

Abstract

In this study, the seismic performance of a rotational friction damper with restoring force is presented. The torsional spring friction damper consists of rotational friction pads with the heavy duty torsional springs attached on both sides of the friction damper. An analytical model and a design procedure for the damper are developed using capacity spectrum method. A parametric study is carried out to investigate the influence of the torsional spring in the response of the structure when subjected to ground motions. The seismic performances of steel structures retrofitted with the torsional spring friction damper and conventional rotational friction dampers are evaluated using fragility analysis, which shows that the structure retrofitted with the torsional spring friction damper has the smallest probability of reaching the specific limit states.

Keywords

fragility analysis, friction dampers, seismic retrofit, self-centering

Introduction

The demand of passive energy dissipation devices for seismic protection of new and existing structures has been rapidly increasing in recent years. Various types of energy dissipation devices have been developed in the literature. For example, displacement-dependent hysteretic devices (Kim et al., 2009; Lee and Kim, 2017; Whittaker et al., 1991), viscous or viscoelastic devices (Javidan and Kim, 2020; Kim and Bang, 2003; Xu et al., 2020, 2003a, Kim et al., 2016), friction devices (Javidan and Kim, 2019; Lee et al., 2008; Mualla and Belev, 2002), and magnetorheological dampers (Xu et al., 2003b; Xu and Shen, 2003) have been widely investigated. One of the drawbacks of using passive dampers for seismic protection is the presence of residual deformation in a structure when subjected to severe ground motions. Residual deformation may result in loss of operational efficiency of the structure, and can also significantly increase repair cost and downtime.

To enhance seismic performance of passive damping devices, hybrid dampers and self-centering dissipative devices have been extensively studied. Self-centering dissipation devices have advantage over conventional passive dampers and stiffening of structures in that the structure can return to its original position after subjected to a ground motion. To reduce or eliminate residual deformation in structures, many researchers have investigated various self-centering retrofitting schemes. For instance, application of post-tensioning re-centering systems to the precast structure have been studied by Priestley et al. (1999) and bracing systems providing energy dissipation capacity and restoring force have been developed (Chou et al., 2016; Christopoulos et al., 2008; Miller et al., 2012). Post-tensioned tendons have been used in pre-stressed precast shear walls, reinforced concrete moment frames (Rahman and Sritharan, 2007), and steel-braced frames (Dyanati et al., 2014; Eatherton et al., 2014; Roke and Jeffers, 2012) to provide stiffness and restoring force. The super-elastic property of shape memory alloy has been used to produce damping devices having both energy dissipation and self-centering capability (Dolce and Cardone, 2006; Ingalkar 2014). Naeem et al. (2017) developed the hybrid damper using the superelastic shape memory alloy bars with the

[1]Department of Civil Engineering, BUITEMS, Quetta, Pakistan
[2]Department of Civil and Architectural Engineering, Sungkyunkwan University, Suwon-si, South Korea

Corresponding author:
Jinkoo Kim, Department of Civil and Architectural Engineering, Sungkyunkwan University, Chunchun Dong, Suwon-si 440-746, South Korea.
Email: jkim12@skku.edu

conventional steel slit damper, which not only enhances the seismic performance of the conventional slit damper but also provides the self-centering capability. Recently Noureldin et al. (2018) investigated optimum design procedure of structures retrofitted with slit–friction hybrid dampers.

The rotational friction dampers (FDs) have been proven to be effective in protecting structures against seismic events (Anoushehei et al., 2017; Kim et al., 2011; Mualla and Belev, 2002; Shirkhani et al., 2015). The seismic performance of FDs combined with other passive devices has also been investigated; Lee and Kim (2015) and Lee et al. (2017) developed a hybrid damping devices by combining steel slit and FDs connected in parallel and showed that the hybrid dampers are especially effective in reducing seismic responses for small to medium earthquakes, compared with slit or FDs with the same yield strength. Mirtaheri et al. (2017) studied the effect of main shock–after shock on the residual displacement of buildings equipped with cylindrical frictional dampers.

This study presents the torsional spring friction damper (TSFD), which is economical and easy to manufacture. The TSFD is the combination of the rotational FD, developed by Mualla and Belev (2002), combined with heavy duty torsional springs which provide additional stiffness and re-centering force during seismic excitations. This self-centering capability is expected to lead to smaller maximum and residual displacements compared to conventional rotational FDs. A parametric study is carried out on a three-story steel structure to show the effectiveness of the TSFD compared to the conventional FD. Seismic loss assessment and life-cycle cost estimation of three-story and eight-story steel structures are performed using 22 sets of ground motions to validate the effectiveness of the TSFD.

TSFDs

A TSFD consists of central and external steel plates rotating against each other as shown in Figure 1. There are circular friction disks between the central and external side plates. The high strength bolt connects the steel plates, steel shafts, and friction pads of the damper. The adjustable bolt with hard washers and spring washers provide the constant clamping force to the friction pads and steel plates. Torsional springs are installed on the steel shafts on both sides of the central steel plate. The arms of the torsional springs are restrained by the central and bottom steel plate welded to the side steel plates. The torsional springs are made of high tensile hard drawn (HD) steel or oil-treated commercial steel which can provide the required spring stiffness for the damper. Figure 2 shows the behavior of the TSFD during an earthquake excitation. The central steel plate of the damper is connected to the girder by a hinge as shown in Figure 2 to avoid bending moment during excitation. The side steel plates of the damper are connected to the inverted-V (chevron) bracing consisting of pre-tensioned bar members to avoid the bending due to compression forces. During earthquake excitation, rotation of the friction pads relative to the steel plates dissipate vibration energy, and the two torsional springs attached parallel to the FD provide re-centering forces to the steel plate, bringing the

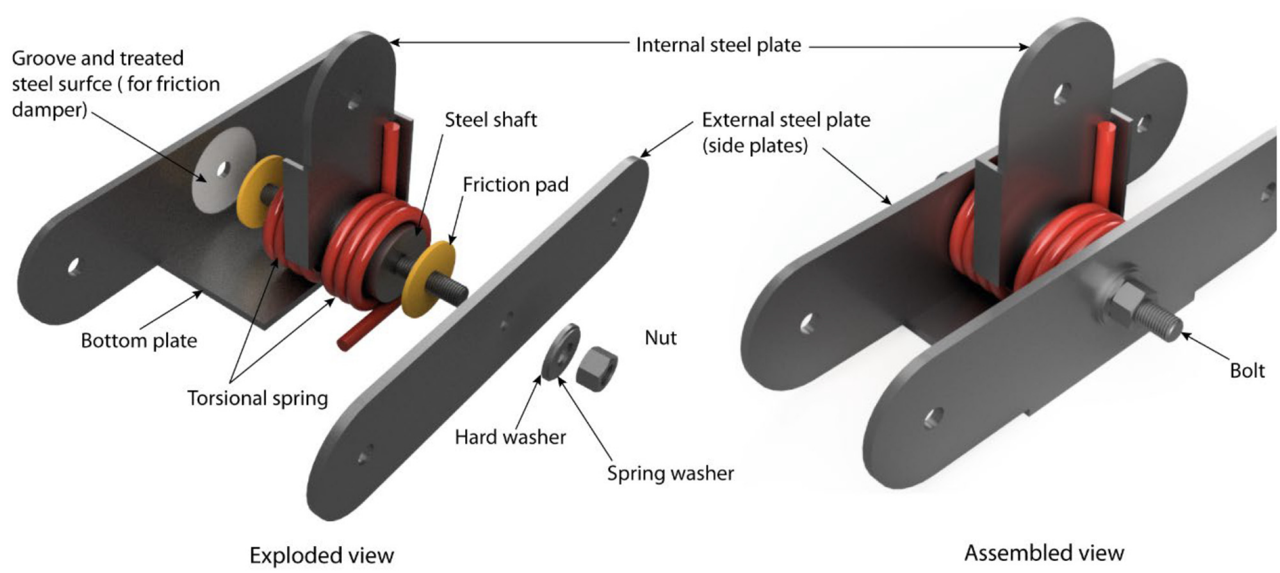

Figure 1. Exploded and assembled view of the torsional spring friction damper (TSFD).

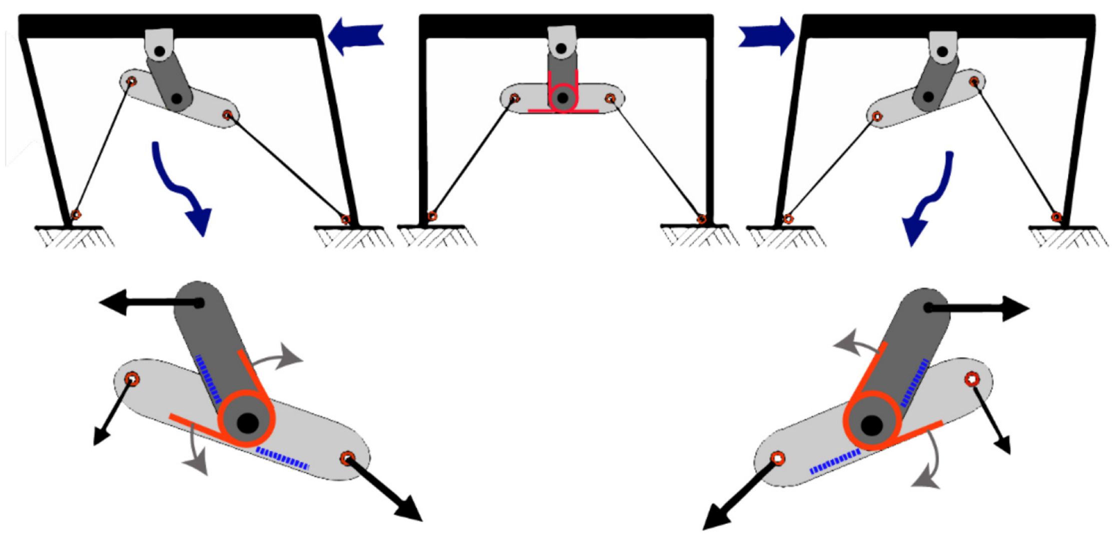

Figure 2. Energy dissipation and re-centering mechanism of the torsional spring friction damper.

damper back to its original position. The torsional springs in the TSFD reduce the residual displacements and enhance the energy dissipation capacity of the FD by providing extra stiffness to the structure.

The FD is activated when the applied load reaches the slip force. As the initial stiffness of a FD is very large, larger energy is dissipated compared with the steel damper with the same yield force. The energy dissipation by the rotational FD is computed by equation (1)

$$u_{\text{dissipated}} = \int_{o}^{t} M_f \left|\dot{\theta}\right| dt \tag{1}$$

where M_f and $\dot{\theta}$ are the rotational strength in the hinge of the damper and the velocity of the hinge's relative rotation, respectively. Figure 3 shows the component forces of a single-story frame equipped with the rotational FD (Mualla and Belev, 2002). The frictional hinge is located at point C, and the slip force of the FD is denoted by F_h. When the external force F_A is exerted on the damper by the beam of the frame, the frictional moment M_f occurs on hinge C, which produces the tension and compression forces in the braces and can be obtained from equation (2)

$$M_f = F2r\sin(v) \tag{2}$$

The axial force in the braces can be calculated by equation (3), where h_a is the length of the vertical steel plate and v is the angle of the braces

$$F_a = \frac{M_f}{2h_a\cos(v)} \tag{3}$$

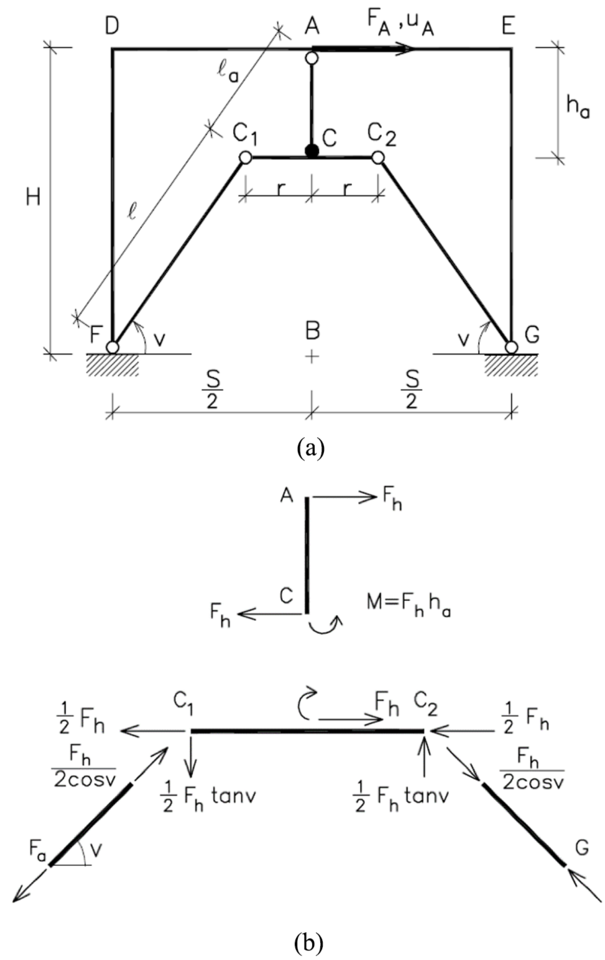

Figure 3. Component forces of the damping system (Mualla and Belev, 2002): (a) analysis model and (b) member forces of damping system.

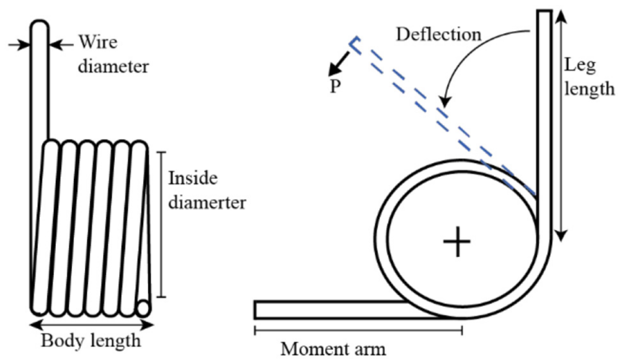

Figure 4. Scheme of the stiffening and re-centering torsional spring details.

The yield force of the FD can be obtained from equation (4), where μ is the friction and coefficient, n is the number of frictional faces, Q is the clamping force of the high tension bolt, l is the length between the plates, and R_m is the effective area of the circular friction face. The friction coefficient of the friction pads is assumed to be 0.35 according to Damptech (2020)

$$F_{\text{yield, friction}} = 2\mu NQ\frac{R_m}{l} \tag{4}$$

Torsional spring exerts the torque when they are deflected, and Figure 4 shows the configuration and behavior of a circular torsional spring. The spring stiffness and force of the torsional spring can be calculated by equations (5) and (6), respectively

$$R = \frac{E \cdot d^4}{10.8DN} \tag{5}$$

$$P = \frac{R \cdot \phi}{m_a} \tag{6}$$

where R is the spring stiffness, E is the modulus of elasticity, d is the wire diameter, N is the number of coils, D is the mean diameter of coils, P is the force of the torsional spring, ϕ is the deflection in degrees, and m_a is the moment arm of the torsional spring.

The nonlinear behavior of the torsional spring FD can easily be developed in the general purpose structural analysis software such as SAP2000. The FD with slip force is modeled using the nonlinear link "wen plastic link," and the linear behavior of the rotational spring can be defined using the "multilinear elastic link." A Hook link is provided to limit the damper to work only in stroke range. The analytical model of a TSFD is presented in Figure 5(a) and the force–displacement response of link elements is depicted in Figure 5(b).

Seismic performance evaluation of retrofitted structures

To investigate the influence of the torsional spring in the TSFD, a parametric study is conducted using analysis model structures. A three- and an eight-story steel moment frames with 6000 mm span length and 4000 mm story height are used as representative models. The model structures are designed considering only the gravity loads under the assumption that they were designed before the seismic codes were enforced; therefore the seismic load is not considered in the structural design and the dead and live loads of 5.0 and 2.5 kN/m^2, respectively, are used as gravity loads. The plan, elevation, and member sizes of the prototype structures are shown in Figure 6, and only one of the exterior frames is separated from each structure for the analysis. The locations of the dampers are also shown in this figure. Beams and columns of the structures are W-shaped sections. Figure 7 shows the stress–strain relationship of the steel used for structural elements, where the material properties of A-36 (ASTM) steel with yield stress of 250 MPa is used for beams and A-572 steel with yield stress of 345 MPa is used for columns.

To carry out nonlinear dynamic analysis of the model structures, the material model of the structural members recommended by the FEMA-356 (2000) is used. Plastic hinges are introduced at the end of the elements to account for the inelastic behavior. Figure 8(a) shows the bending moment *versus* rotation angle relationship of the flexural members. The coefficients used to define the nonlinear behavior (a, b, and c) are computed considering the width–thickness ratios of the structural members. Figure 8(b) indicates the deformation levels corresponding to each performance point such as the first yield, immediate occupancy (IO), life safety (LS), collapse prevention (CP), collapse, and fracture as specified in the FEMA-356. The inherent damping ratio of the structure is assumed to be 3% of the critical damping.

The three-story bare frame is subjected to seven earthquakes shown in Table 1 which are scaled to design level response spectrum of Los Angeles as shown in Figure 9. The maximum inter-story drift ratio (MIDR) and the maximum roof displacement (MRD) of the structure are shown in Figure 10. The MIDR is obtained to check whether the code-specified limit state is satisfied, and MRD is obtained to show the global behavior of the structure. It can be observed that the mean MIDR is 2.90% of the story height. In this study the limit state for the design level earthquake is set to be 1.5% of the story height (Korea Building Code (KBC), 2019), and the maximum inter-story drift response of the model structure turns out to exceed this limit state. The mean residual and MRD of

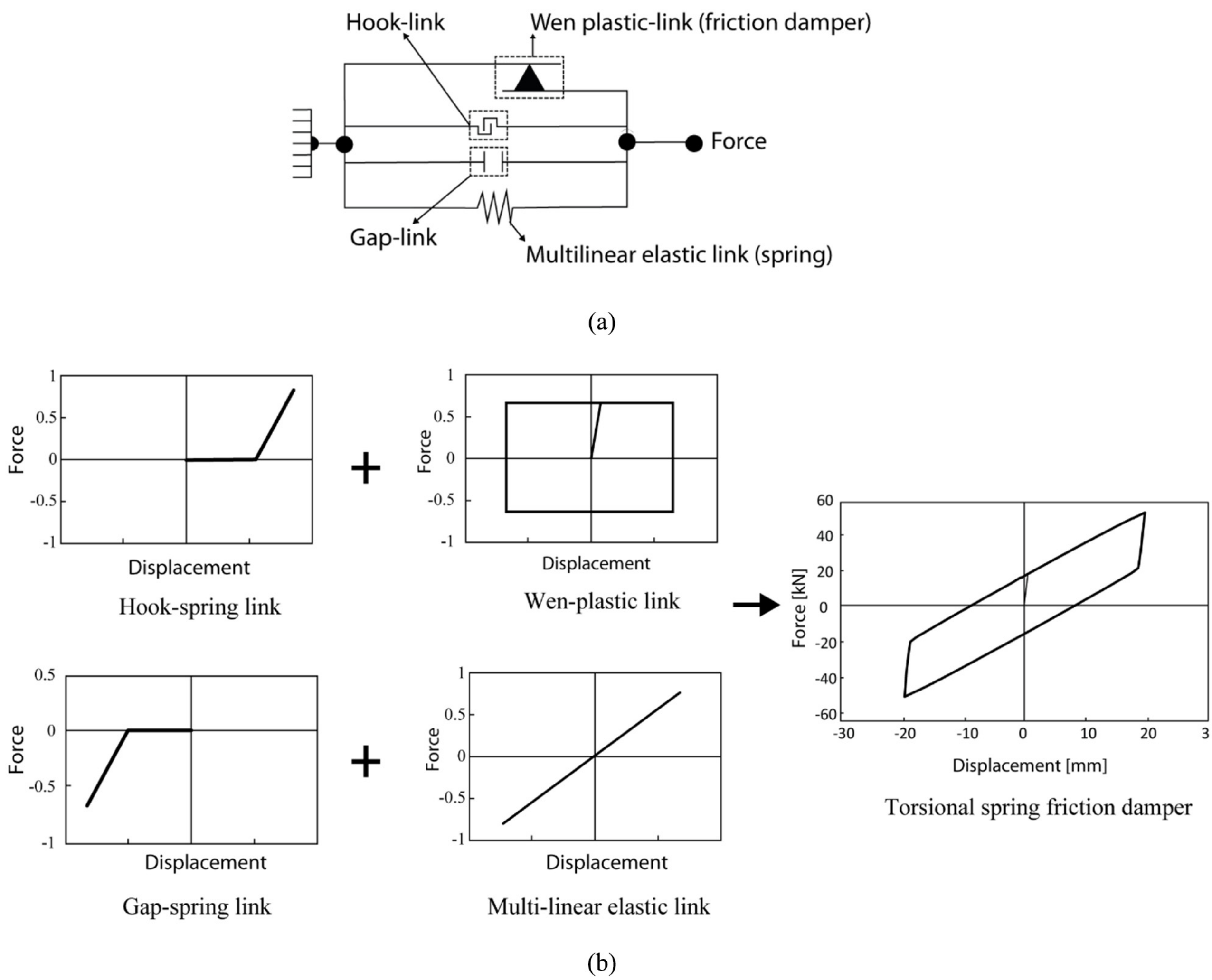

Figure 5. Analytical model developed for the torsional spring FD: (a) assembly of link elements and (b) force–displacement relationships of the link elements.

the structure are 57 and 282 mm, respectively, for the seven ground motions.

In the first part of this parametric study, the structure is retrofitted with the conventional FD to investigate the effect of the friction force. Nonlinear time history analyses of the model structure installed with FDs are performed using the selected seven earthquakes, and the mean MIDR, MRD, and the residual displacements are plotted in Figure 11. It can be observed that the MIDR and MRD of the structure keep decreasing as the slip force of the FDs keeps increasing. However, the rate of reduction becomes marginal after the friction force is increased over about 80 kN. This may be due to the fact that as the friction force becomes larger and larger the damping system acts more and more like a tension-only bracing. The residual displacement of the structure rather increases as the slip force exceeds that value. It can be observed that the inter-story drift limit state of 1.5% of the story height is satisfied as the slip force increases higher than about 40 kN.

Similar analyses are performed for the structure retrofitted with the TSFD to examine the influence of the stiffness and the restoring force of the torsional spring. The torsional spring stiffness of the TSFD is varied from 5 to 40 kN-mm/deg (commercially available range) with four different slip forces (25, 50, 100, and 160 kN) of the FD. Figure 12(a) shows the mean MIDR of the seven analyses for the TSFD variable spring stiffness (5, 10, 15, 20, 25, 30, and 40 kN-mm/deg). The results show that as the spring stiffness increases the structural responses generally decreases. It also can be observed that the effect of the spring stiffness decreases as the slip force of the FD decreases. The rate of decrease in the inter-story and roof displacements is slowed down as the spring stiffness

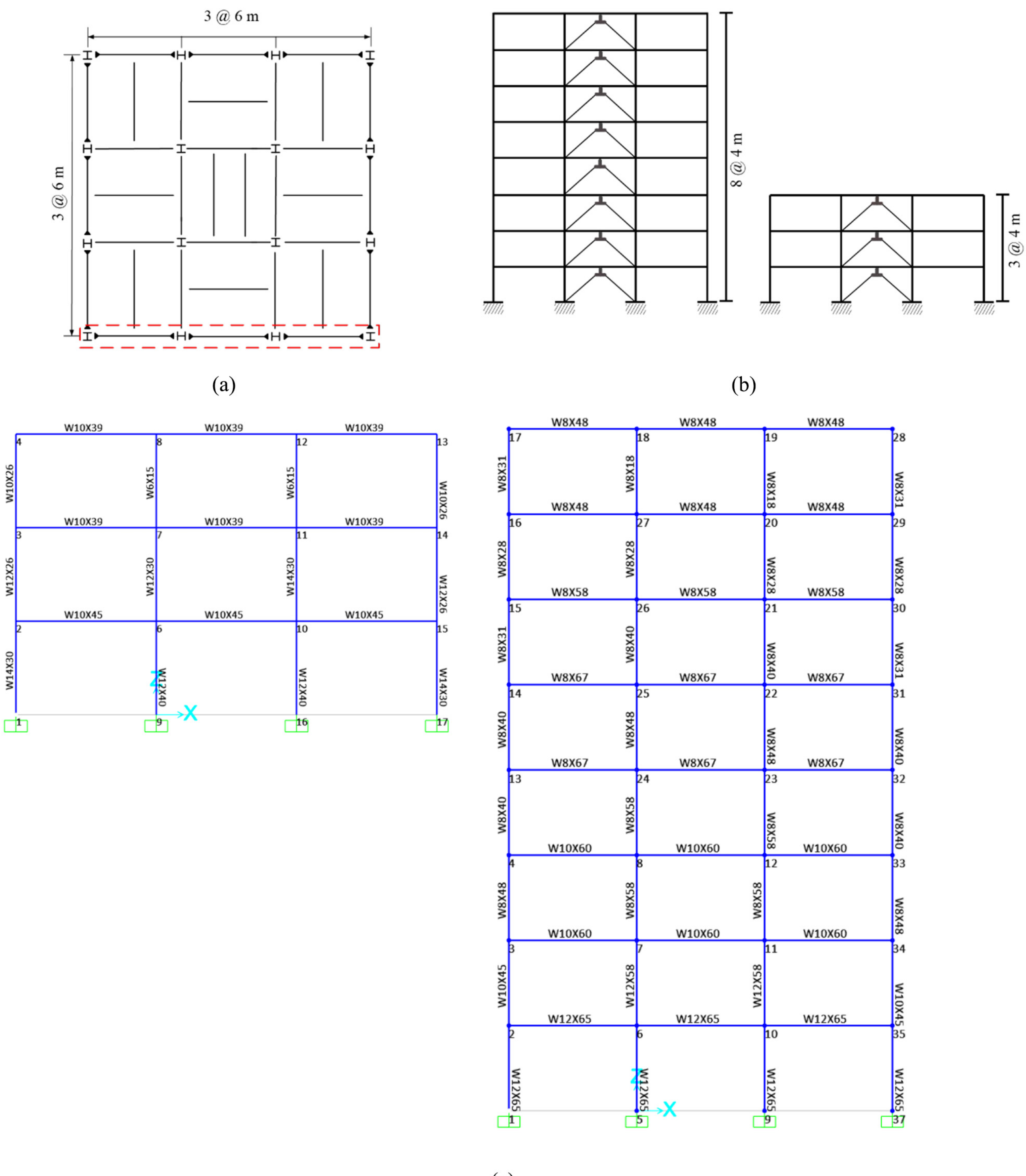

Figure 6. Analysis model steel structures: (a) structural plan, (b) elevation, and (c) member size of structural elements.

increases, and as the spring stiffness increases higher than 25 kN-mm/deg, the residual displacement rather increases.

The seismic performance of the model structures is investigated by performing nonlinear time history analysis using the earthquake records provided by PEER NGA data base. The selected ground motion records are from large magnitude events and recorded at moderate fault-rupture distances on stiff soil or rock sites. The model structures are assumed to be located in the south of Los Angeles with spectral acceleration parameters $S_{DS} = 1.4g$ and $S_{D1} = 0.7$ g. The dampers are

Table 1. Earthquake records used for dynamic analysis.

ID no.	Record no.	Earthquake name	Component	Distance (km)	PGA (g)
1	174	Imperial Valley	IMPVALL/H-EI1230		0.38
2	68	San Fernando	SFERN/PEL180		0.21
3	721	Superstition hills	SUPERST/B-ICC000		0.36
4	752	Loma Prieta	LOMAP/CAP000		0.53
5	953	Northridge	NORTHR/MUL009	320	0.52
6	1111	Kobe Japan	KOBE/MIS000	>500	0.51
7	1485	Chi-Chi	CHICHI/CHY101-E	>500	0.44

PGA: peak ground acceleration.

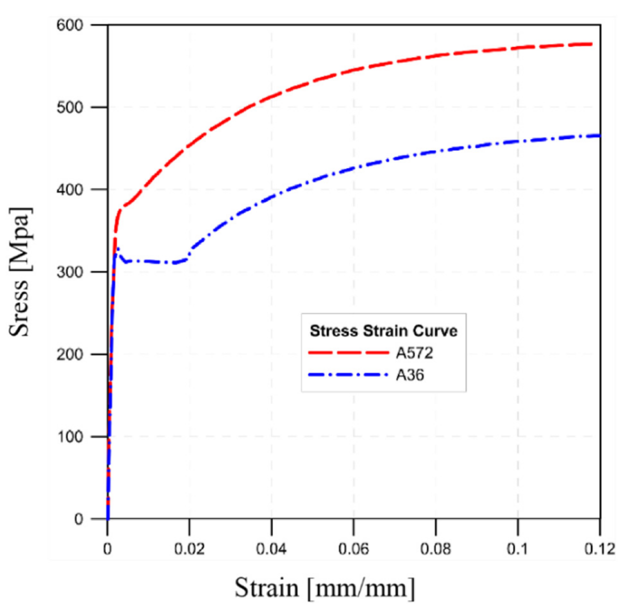

Figure 7. Stress–strain relationship of steel material.

placed in the center bay as shown in Figure 6 (b). The TSFDs are designed with smaller slip force than FD. Table 2 shows the damper force and spring stiffness applied in the model structures. The engineering demand parameters for evaluating the seismic performance are the MIDR and the MRD. Figure 13 shows the roof displacement time histories of the three-story structure before and after the seismic retrofit subjected to four selected ground motions. The FD applied for the retrofit has slip force of 40 kN, and the TSFD has 20 kN slip force, and 25 kN-mm/deg spring stiffness. It can be observed that the maximum displacement of the model structure decreases significantly after placement of the dampers, and that the residual displacement at the end of the seven earthquakes is minimum in the structure retrofitted with the TSFD, even though the slip force used for TSFD is only a half of what is used for the FD. The histograms in Figures 14 to 16 depict the analysis results of 22 ground motions in terms of the MRD, MIDR, and mean residual displacement of the structures before and after the retrofit. It

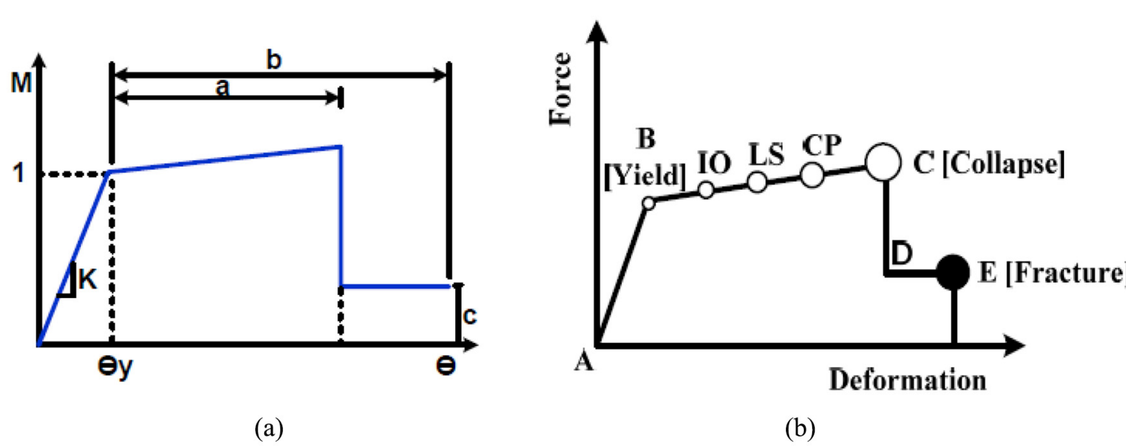

Figure 8. Nonlinear modeling of flexural members: (a) moment–rotation relationship and (b) definition of performance points.

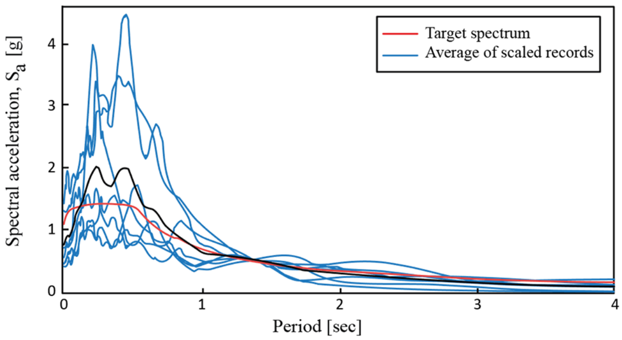

Figure 9. Response spectra of the seven ground motions and the target design spectrum.

can be observed that marginal difference exists in the maximum displacements of the model structures retrofitted with the two different dampers. The structures retrofitted with the TSFD show lower MIDR compared to the structures retrofitted with the FD for most of the earthquakes. It is observed that in the three-story structures the mean inter-story drift ratio is 0.75% and 1.20% for the TSFD and FD retrofit, respectively. A similar trend is also observed in the eight-story structure, where the mean maximum displacement of 295 mm in the bare structure is reduced to 165 mm in the structure with FD, and is further reduced to 140 mm in the structure with TSFD. The mean MIDR of the eight-story structure with TSFD is 0.83%, which is the smallest in all eight-story structures. Similar trend can be noticed in the residual displacements. It is observed that in the bare structure plastic hinges form at the third-story columns. The beams remain elastic due to composite action with the reinforced concrete slabs. It is also noticed that no plastic hinge is formed in the structure retrofitted with FD or TSFD.

Probability of reaching limit states

In this section, the safety assessment of the model structures retrofitted with the FD and TSFD is conducted based on a probabilistic approach using fragility analysis. A seismic fragility curve shows the probability that the response of a structure exceeds a specific limit state when subjected to a ground motion with a specified intensity. The risk assessments of the structures retrofitted with the TSFD and the FD are carried out and the results are compared to those of the model structure before the retrofit. The fragility analysis is carried out using 22 pairs of far field ground motion records provided in the PEER-NGA database (PEER 2017). The seismic fragility is described by the conditional probability that the structural capacity C fails to resist the structural demand D, given the seismic intensity, SI. The fragility function can be well fitted to a lognormal cumulative distribution function as follows (Celik and Ellingwood, 2009)

$$P[C<D|SI=x]=1-\Phi\left[\frac{\ln\left(\frac{\hat{C}}{\hat{D}}\right)}{\sqrt{\beta_{D/SI}^2+\beta_C^2+\beta_M^2}}\right]=1-\Phi\left[\ln\frac{\left(\frac{\hat{C}}{\hat{D}}\right)}{\beta_{TOT}}\right] \tag{7}$$

where $\Phi[\cdot]$ is the standard normal cumulative distribution function, $\hat{C}$ is the median structural capacity associated with the limit state, and $\hat{D}$ is the median structural demand. The uncertainties in seismic risk assessment are considered using the uncertainty in the capacity β_C, uncertainty in the structural demand $\beta_{D/SI}$, and modeling uncertainties β_M. In this study, the total system collapse uncertainty β_{TOT} is assumed to be 0.6 according to FEMA P695 (Federal Emergency Management Agency (FEMA) 2009) throughout this study.

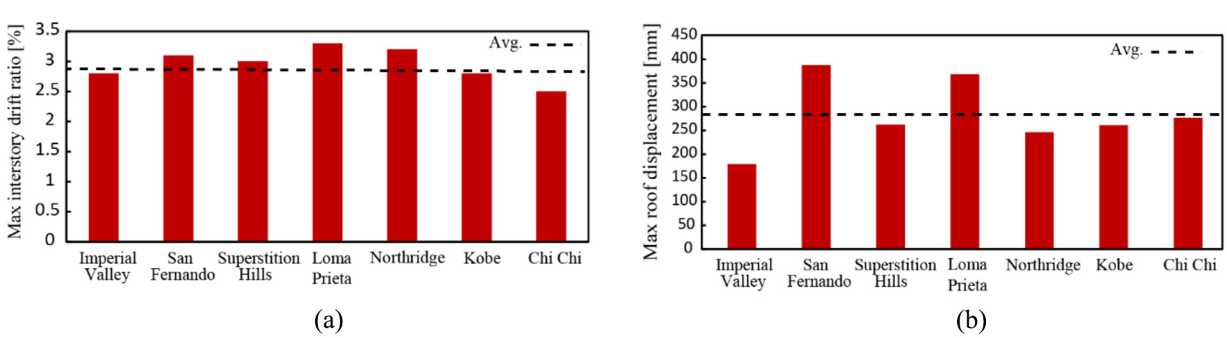

Figure 10. Response of three-story bare structure subjected to seven ground motions: (a) inter-story drift ratio and (b) maximum roof displacement.

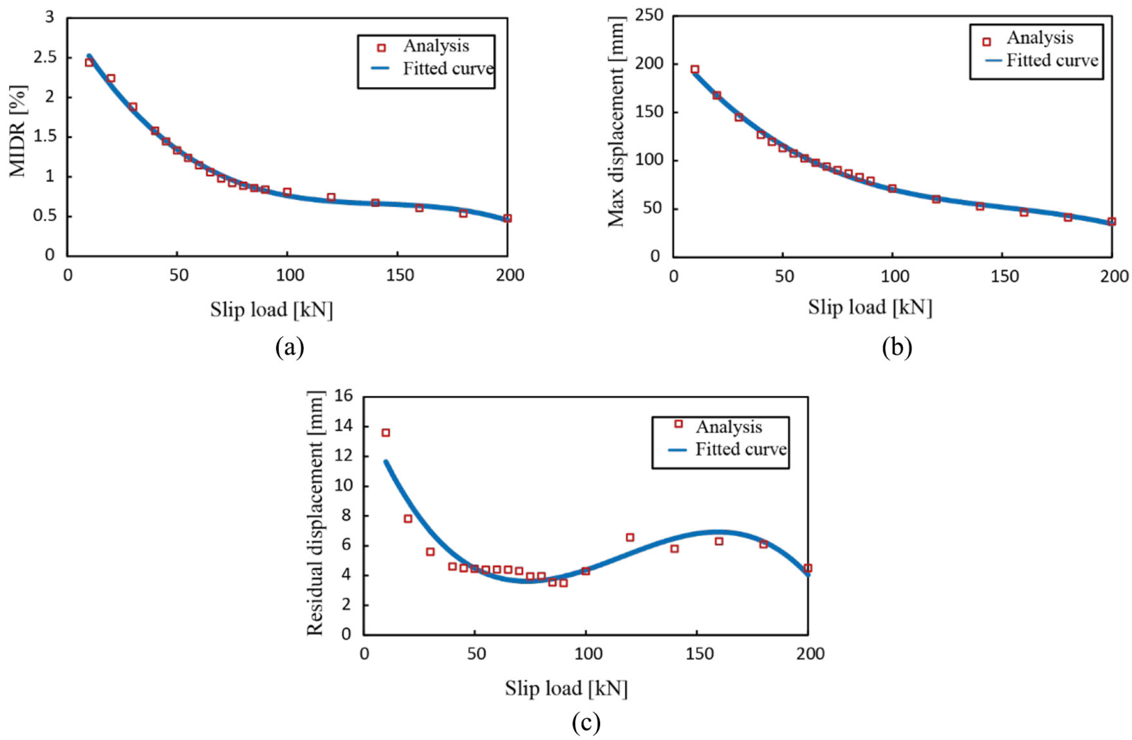

Figure 11. Response of the three-story structure retrofitted with conventional rotational friction dampers (FD) with varying slip force: (a) maximum inter-story drift ratios (MIDRs), (b) maximum displacements, and (c) residual displacements.

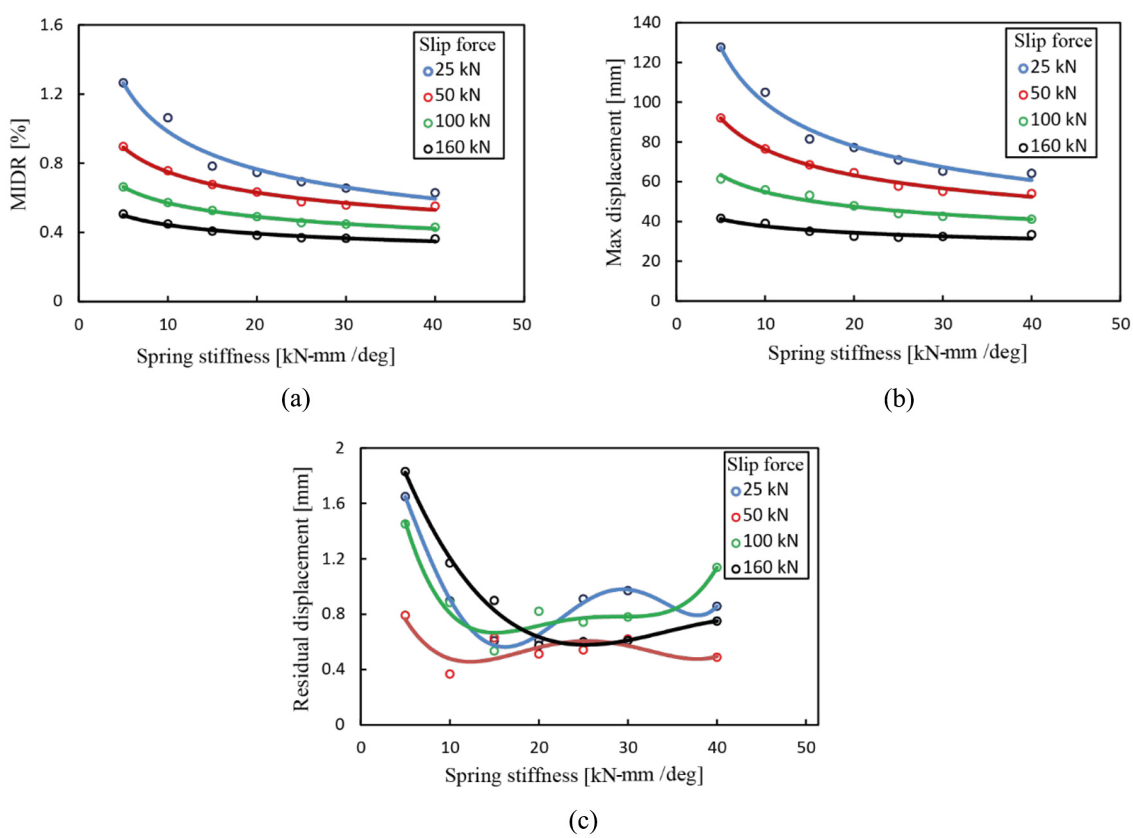

Figure 12. Response of the three-story structure retrofitted with TSFD with varying spring stiffness: (a) mean maximum inter-story drift, (b) maximum roof displacement, and (c) residual displacement of structure.

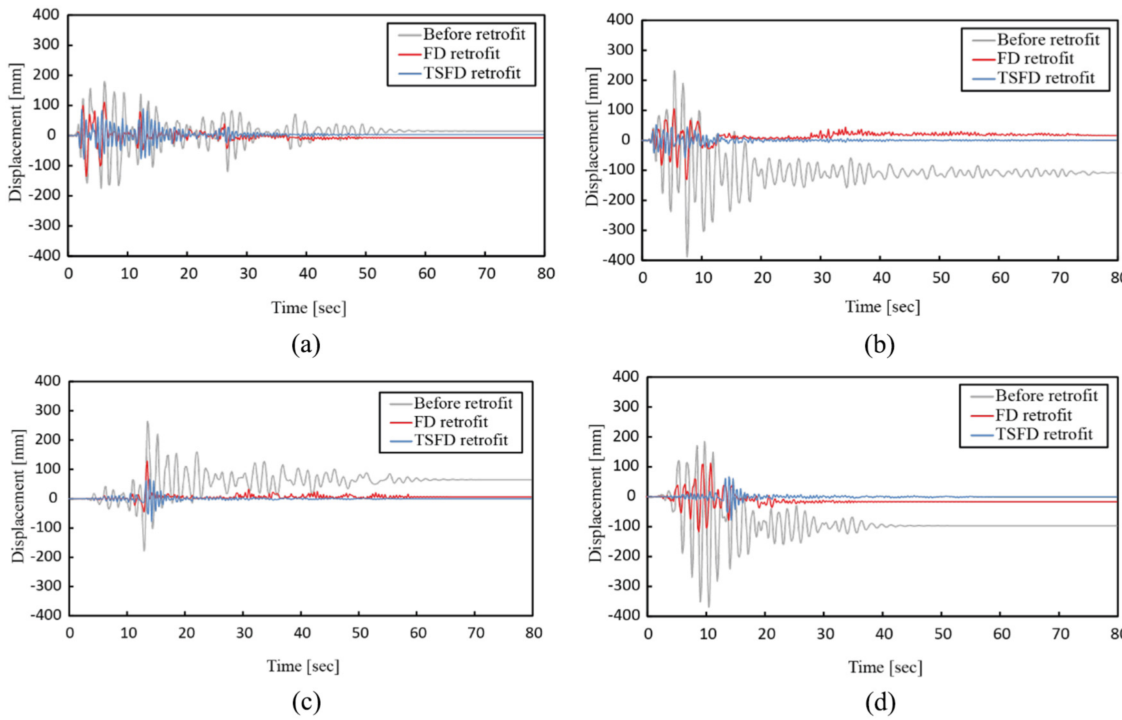

Figure 13. Roof displacement time histories of the three-story structure before and after retrofit subjected to selected earthquake records: (a) Imperial Valley (El Centro), (b) San Fernando, (c) Superstition Hills, and (d) Loma Prieta.

Table 2. Damping forces of the FD and TSFD applied to the model structures.

Model	FD	TSFD	
	Slip force (kN)	Slip force (kN)	Spring stiffness (kN/mm)
Three-story	40	20	25
Eight-story	90	45	30

FD: friction damper; TSFD: torsional spring friction damper.

To obtain fragility curves of the model structures, incremental dynamic analyses (IDAs) of the structures before and after the retrofit are carried out first using the 22 pairs of earthquake records and the statistical distribution of the dynamic response is obtained. The ground motion records are scaled incrementally as recommended in Vamvatsikos and Cornell (2002) for IDA. The scaling factors of the earthquake records are increased till a story or a number of stories displace sufficiently and the first-order story shear resistance becomes zero (i.e. dynamic instability occurs). The slip force and the spring stiffness of the dampers applied to the model structures along with their natural periods are summarized in Table 3. For comparison purpose, the structures are retrofitted with the TSFD with 50% and 100% of the slip force used for FD. Figure 17 shows the spectral acceleration *versus* MIDRs obtained from IDA of the three-story structures before and after the retrofit. In Table 4 the median spectral acceleration for the 22 ground motions corresponding to the limit states are also shown. It can be observed that, for a given spectral acceleration, the inter-story drift of the structure decreases after retrofitting with the TSFD and FD. It also can be noticed that, for a given inter-story drift ratio, the median value is highest in the structure retrofitted with TSFD with 100% slip force.

Based on the IDA results the probability of reaching the limit states and the corresponding fragility curves can be drawn for various damage states. In HAZUS (1997) damage states are defined in the four different stages which are slight, moderate, extensive, and complete damages. The slight damage is defined as the state with minute cracks, and the moderate damage is the state with formation of widely spread cracks with partial yielding. In the extensive damage state part of the structure has reached ultimate states, and in the complete damage state the structure is near collapse. In this study the probability of reaching three different limit states such as IO, LS, and CP are computed. The corresponding inter-story drift ratios for the three limit states are 1.0%, 1.5%, and 2.5% of the story height, respectively. Figures 18 and 19 present the fragility curves for the three-story and eight-story model structures, respectively, corresponding to the three different

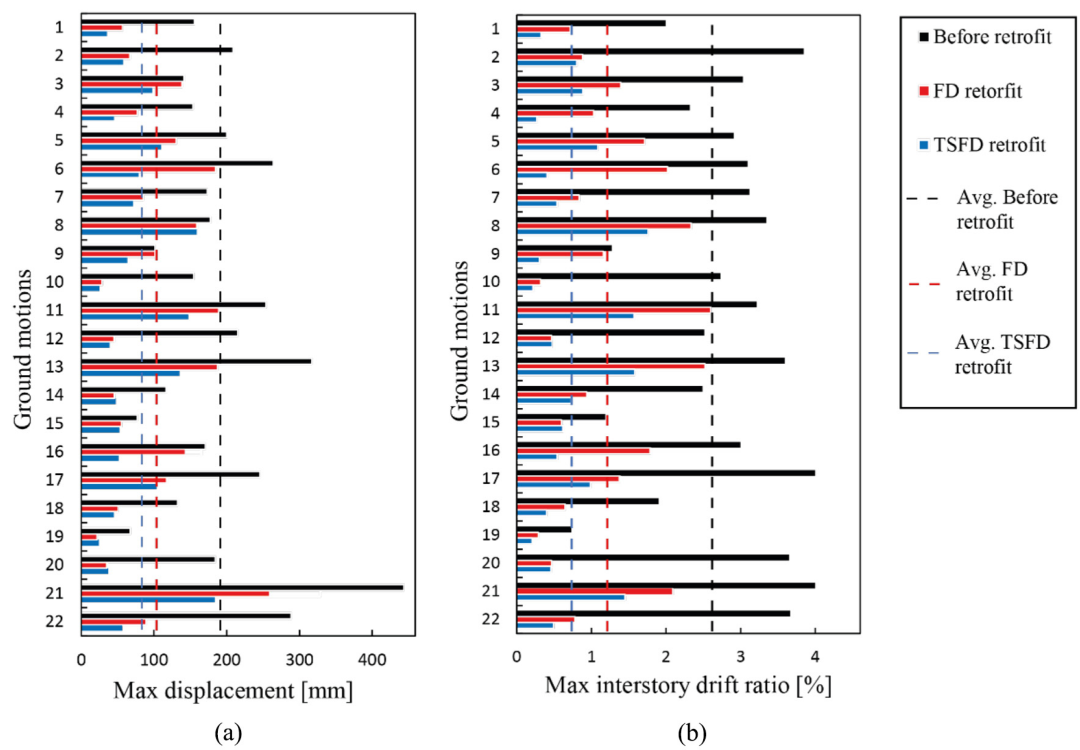

Figure 14. Responses of the three-story structure subjected to 22 ground motions: (a) maximum roof displacement and (b) maximum inter-story drift ratio.

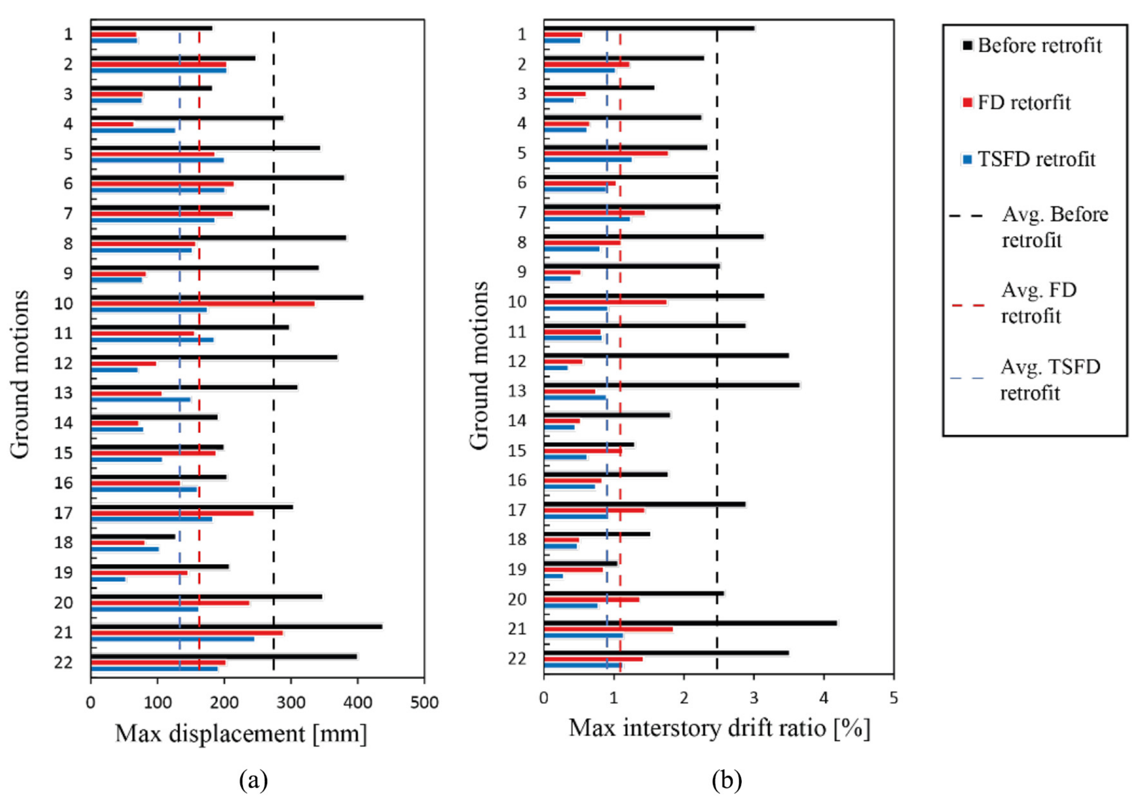

Figure 15. Responses of the eight-story structure subjected to 22 ground motions: (a) maximum roof displacement and (b) maximum inter-story drift ratio.

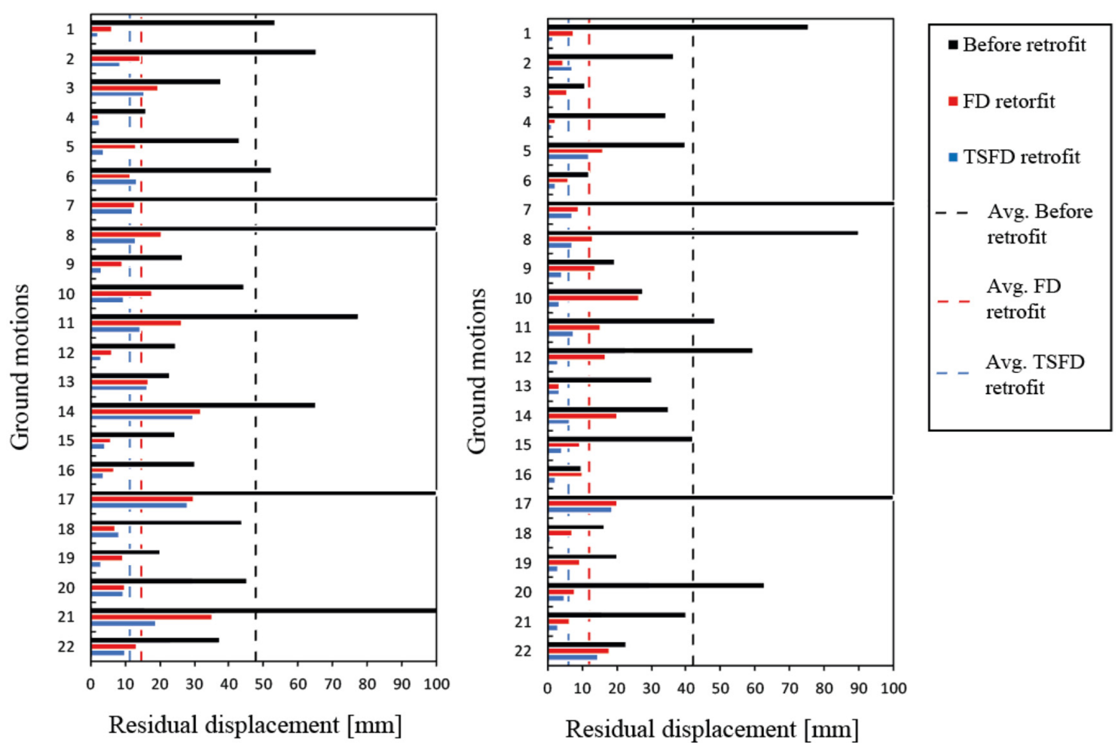

Figure 16. Residual displacement of three-story and eight-story structure subjected to 22 ground motions.

Table 3. Natural periods of model structures.

Story	Model name	FD	TSFD		T_n
		Slip force (kN)	Slip force (kN)	Spring stiffness (kN/mm)	(s)
Three	3-Bare frame	–	–	–	1.40
	3-FD	40	–	–	0.56
	3-TSFD (50%)	–	20	25	0.53
	3-TSFD (100%)		40	25	0.47
Eight	8-Bare frame	–	–	–	2.70
	8-FD	90	–	–	1.20
	8-TSFD (50%)	–	45	30	1.16
	8-TSFD (100%)	–	90	30	1.05

FD: friction damper; TSFD: torsional spring friction damper.

Table 4. Median collapse intensities of model structures.

Story	Limit states	Before retrofit	FD retrofit	TSFD (50%) retrofit	TSFD (100%) retrofit
Three	IO	0.182 g	0.790 g	1.066 g	1.184 g
	LS	0.275 g	0.982 g	1.254 g	1.432 g
	CP	0.425 g	1.303 g	1.561 g	1.786 g
Eight	IO	0.202 g	0.577 g	0.607 g	0.819 g
	LS	0.247 g	0.795 g	0.810 g	1.127 g
	CP	0.322 g	1.121 g	0.998 g	1.285 g

FD: friction damper; TSFD: torsional spring friction damper; IO: immediate occupancy; LS: life safety; CP: collapse prevention.

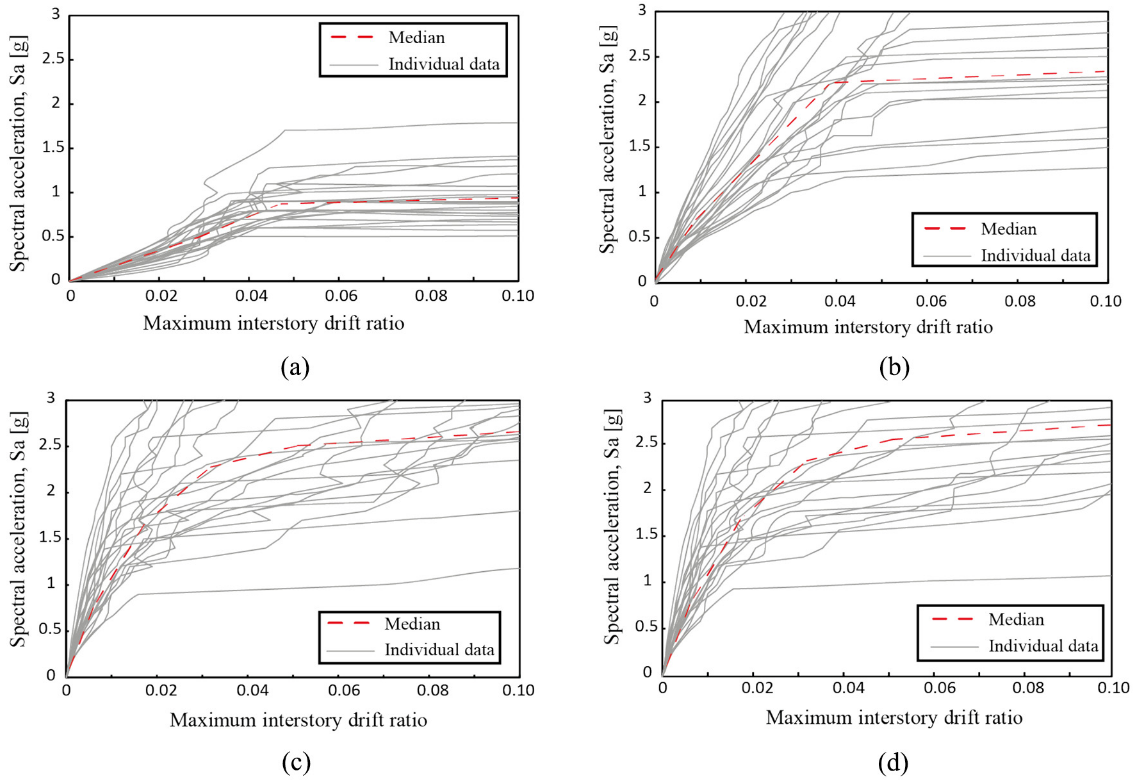

Figure 17. Incremental dynamic analysis results of the three-story structure before and after retrofit: (a) before retrofit, (b) FD retrofit, (c) TSFD (50%) retrofit, and (d) TSFD (100%) retrofit.

limit states before and after the retrofit. The fragility curves show that the probability of reaching the limit states is largest in the bare frame and is decreased in the retrofitted structures, which denotes that the dampers are effective in decreasing the failure probability of the structure against seismic events. Fragility curves clearly demonstrate the effectiveness of the TSFD over the FD: The structures retrofitted with the TSFD having 100% of the slip force have the mean failure probability approximately 23.5% and 38.5% smaller than those of the structures retrofitted with FD for the IO and LS limit states, respectively. For the CP limit state, the average percentage reduction is 52%. Even the structures retrofitted with the TSFD with 50% of the slip force show smaller probability of reaching the limit state than the structures with the FD except for the eight-story structure corresponding to the CP limit state.

The difference in the probabilities of failure of the TSFD and FD retrofit systems is more pronounced in the three-story structure. Due to the limitation in the stiffness of torsional spring available in the market, the TSFD will be more effective in low to mid-rise structures.

Summary and conclusion

In this study, a FD with a restoring force was developed by combining a torsional spring and a rotational FD. To investigate the efficiency of the proposed system, three- and eight-story steel structures were retrofitted with the TSFD and the typical rotational FDs having the same friction force, and their seismic performances were compared. Parametric studies were carried out to investigate the effectiveness of the springs used in combination with the FDs. Fragility analyses were conducted to compute the probability of reaching given limit states, and the cost effectiveness of the torsional spring FDs was investigated by evaluation of life cycle costs.

The analysis results showed that both the maximum and residual displacements were reduced after implementing torsional springs to FDs. The TSFD with 50% slip force of the FD resulted in better seismic performance of the model structures compared to the FD with 100% slip force. The probabilities of reaching limit states and the life cycle costs were minimized by the seismic retrofit with the TSFD. The overall analysis results showed that combining torsional springs with

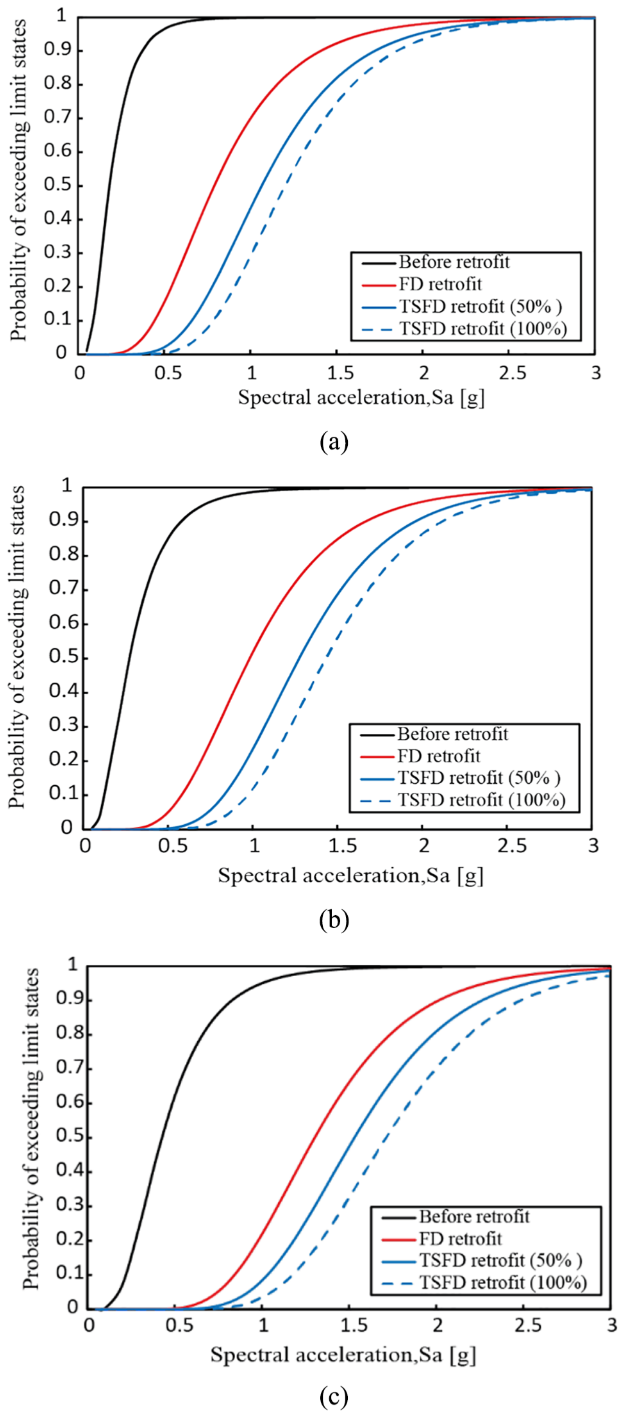

Figure 18. Fragility curves of the three-story structure: (a) immediate occupancy, (b) life safety, and (c) collapse prevention.

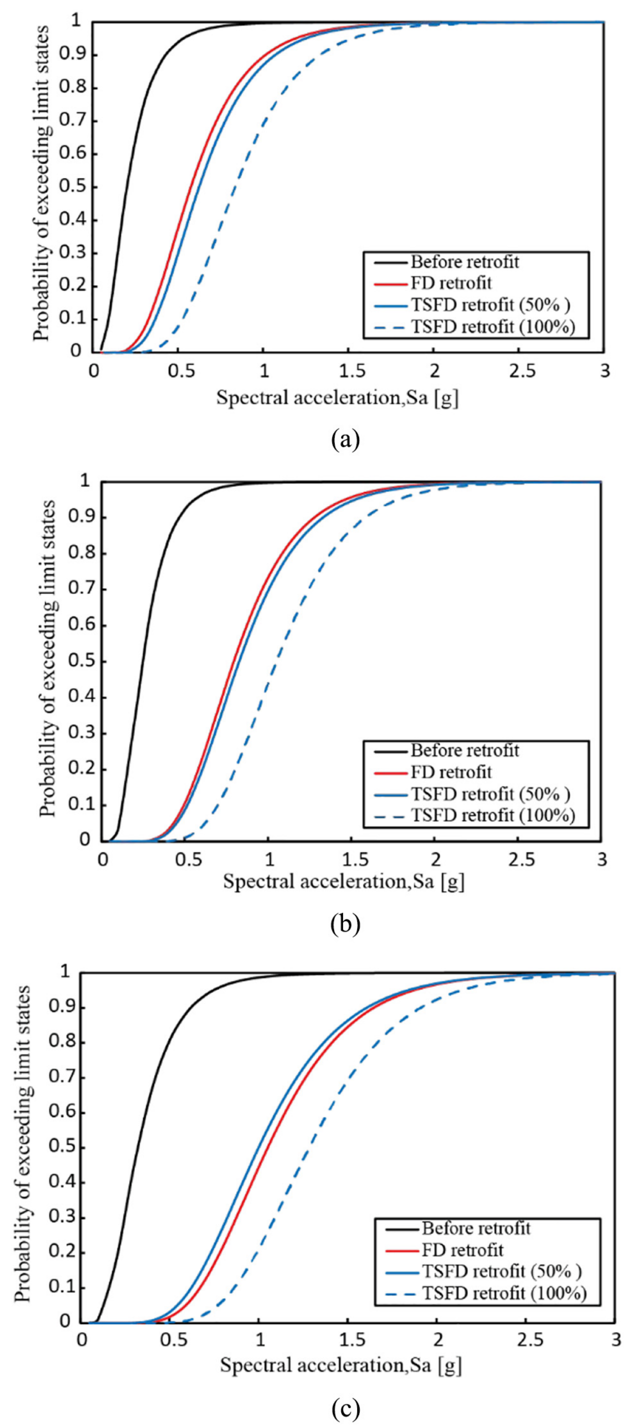

Figure 19. Fragility curves of the eight-story structure: (a) immediate occupancy, (b) life safety, and (c) collapse prevention.

rotational friction dampers was effective in increasing seismic performance and cost-effectiveness of conventional dampers.

Declaration of Conflicting Interests

The author(s) declared no potential conflicts of interest with respect to the research, authorship, and/or publication of this article.

Funding

The author(s) disclosed receipt of the following financial support for the research, authorship, and/or publication of this article: This research was carried out by research funding (task number: 19CTAP-C153076-01) of the Ministry of Land, Infrastructure and Transport, Land Transport Technology Promotion Research Project.

ORCID iD

Jinkoo Kim https://orcid.org/0000-0002-3605-8189

References

Anoushehei M, Daneshjoo F, Mahboubi S, et al. (2017) Experimental investigation on hysteretic behavior of rotational friction dampers with new friction materials. *Steel and Composite Structures* 24(2): 239–248.

Celik OC and Ellingwood BR (2009) Seismic risk assessment of gravity load designed reinforced concrete frames subjected to Mid-America ground motions. *Journal of Structural Engineering* 135(4): 414–424.

Chou CC, Tsai WJ and Chung PT (2016) Development and validation tests of a dual-core self-centering sandwiched buckling-restrained brace (SC-SBRB) for seismic resistance. *Engineering Structures* 121: 30–41.

Christopoulos C, Tremblay R, Kim HJ, et al. (2008) Self-centering energy dissipative bracing system for the seismic resistance of structures: development and validation. *Journal of Structural Engineering* 134(1): 96–107.

Damptech (2020). Available at: www.damptech.com/downloads.html

Dolce M and Cardone D (2006) Theoretical and experimental studies for the application of shape memory alloys in civil engineering. *Journal of Engineering Materials and Technology* 128(3): 302–311.

Dyanati M, Huang Q and Roke DA (2014) Structural and nonstructural performance evaluation of self-centering, concentrically braced frames under seismic loading. In: *Structures Congress*, pp. 2393–2404.

Eatherton MR, Ma X, Krawinkler H, et al. (2014) Design concepts for controlled rocking of self-centering steel-braced frames. *Journal of Structural Engineering* 140(11): 04014082.

Federal Emergency Management Agency (FEMA) (2009) *Quantification of Building Seismic Performance Factors* (FEMA P695). Washington, DC: FEMA.

FEMA (2000) FEMA *356: Prestandard and commentary for the seismic rehabilitation of buildings*. Washington, DC, USA: Federal Emergency Management Agency.

HAZUS (1997). *Multi-hazard Loss Estimation Methodology: User Manual*. Washington, DC: Federal Emergency Management Agency.

Ingalkar RS (2014) Rehabilitation of buildings and bridges by using Shape Memory Alloys (SMA). *International Journal of Civil Engineering Research* 5(2): 163–168.

Javidan MM and Kim J (2019) Seismic retrofit of soft-first-story structures using rotational friction dampers. *Journal of Structural Engineering* 145(12): 04019162.

Javidan MM and Kim J (2020) Experimental and numerical sensitivity assessment of viscoelasticity for polymer composite materials. *Scientific Reports* 10(1): 675.

Korea Building Code (KBC) (2019) *Architectural Institute of Korea*. Seoul, South Korea: KBC.

Kim J and Bang S (2003) Optimum distribution of added VED for mitigation of torsional responses of plan-wise asymmetric structures. *Engineering Structures* 24(10): 257–269.

Kim J, Choi H and Min KW (2011) Use of rotational friction dampers to enhance seismic and progressive collapse resisting capacity of structures. *The Structural Design of Tall and Special Buildings* 20(4): 515–537.

Kim J, Lee J and Kang H (2016) Seismic retrofit of special truss moment frames using viscous dampers. *Journal of Constructional Steel Research* 123: 53–67.

Kim J, Park J and Kim SD (2009) Seismic behavior factors of buckling-restrained braced frames. *Structural Engineering and Mechanics* 33(3): 261–284.

Lee J and Kim J (2015) Seismic performance evaluation of moment frames with slit-friction hybrid dampers. *Earthquakes and Structures* 96(6): 1291–1311.

Lee J and Kim J (2017) Development of Steel Box-shaped slit dampers for Seismic Retrofit of building structures. *Engineering Structures* 150: 934–946.

Lee J, Kang H and Kim J (2017) Seismic performance of steel plate slit-friction hybrid dampers. *Journal of Constructional Steel Research* 136: 128–139.

Lee SK, Park JH, Moon BW, et al. (2008) Design of a bracing -friction damper system for seismic retrofitting. *Smart Structures and Systems* 4(5): 685–696.

Miller DJ, Fahnestock LA and Eatherton MR (2012) Development and experimental validation of a nickel–titanium shape memory alloy self-centering buckling-restrained brace. *Engineering Structures* 40: 288–298.

Mirtaheri M, Amini M and Doosti Rad M (2017) The effect of mainshock-aftershock on the residual displacement of buildings equipped with cylindrical frictional damper. *Earthquakes and Structures* 12(5): 515–527.

Mualla IH and Belev B (2002) Performance of steel frames with a new friction damper device under earthquake excitation. *Engineering Structures* 24(3): 365–371.

Naeem A, Eldin MN, Kim J, et al. (2017) Seismic performance evaluation of a structure retrofitted using steel slit dampers with shape memory alloy bars. *International Journal of Steel Structures* 17(4): 1627–1638.

Noureldin M, Kim J and Kim J (2018) Optimum distribution of steel slit-friction hybrid dampers based on life cycle cost. *Steel and Composite Structures* 27(5): 633–646.

PEER (2017) PEER NGA database. Berkeley, CA: Pacific Earthquake Engineering Research Center, University of California, Berkeley Available at: http://peer.berkeley.edu/nga

Priestley MN, Sritharan S, Conley JR, et al. (1999) Preliminary results and conclusions from the PRESSS five-story precast concrete test building. *PCI Journal* 44(6): 42–67.

Rahman MA and Sritharan S (2007) Performance-based seismic evaluation of two five-story precast concrete hybrid frame buildings. *Journal of Structural Engineering* 133(11): 1489–1500.

Roke D and Jeffers B (2012) Parametric study of self-centering concentrically-braced frame systems with friction-based energy dissipation. In: *Proceeding of Behaviour of Steel Structures in Seismic Areas (STESSA)*, Santiago, Chile, 9–11 January, pp. 691–696. Boca Raton, FL: CRC Press.

Shirkhani A, Mualla IH, Shabakhty NSR, et al. (2015) Behavior of steel frames with rotational friction dampers by endurance time method. *Journal of Constructional Steel Research* 107: 211–222.

Vamvatsikos D and Cornell CA (2002) Incremental dynamic analysis. *Earthquake Engineering & Structural Dynamics* 31(3): 491–514.

Whittaker AS, Bertero VV, Thompson CL, et al. (1991) Seismic testing of steel plate energy dissipation devices. *Earthquake Spectra* 7(4): 563–604.

Xu ZD and Shen YP (2003) Intelligent bi-state control for the structure with magnetorheological dampers. *Journal of Intelligent Material Systems and Structures* 14(1): 35–42.

Xu ZD, Ge T and Liu J (2020) Experimental and theoretical study of high energy dissipation viscoelastic dampers based on acrylate rubber matrix. *Journal of Engineering Mechanics* 146(6). Epub ahead of print. DOI: 10.1061/(ASCE)EM.1943-7889.0001802.

Xu ZD, Shen YP and Zhao HT (2003a) A synthetic optimization analysis method on structures with viscoelastic dampers. *Soil Dynamics and Earthquake Engineering* 23(8): 683–689.

Xu ZD, Shen YP and Guo YQ (2003b) Semi-active control of structures incorporated with magnetorheological dampers using neural networks. *Smart Materials and Structures* 12(1): 80–87.